Reconstruction of energy spectra of elemental groups with KASCADE: sensitivity to hadronic interaction models

H. Ulrich, T. Antoni, W.D. Apel, A.F. Badea*), K. Bekk, J. Blümer, H. Bozdog, K. Daumiller, P. Doll, R. Engel, J. Engler, F. Fessler, H.J. Gils, A. Haungs, D. Heck, H.O. Klages, G. Maier†), H.J. Mathes, H.J. Mayer, J. Milke, M. Müller, R. Obenland, J. Oehlschläger, S. Ostapchenko‡), H. Rebel, M. Risse, G. Schatz, H. Schieler, J. Scholz, T. Thouw, J. van Buren, A. Weindl, J. Wochele

Institut für Kernphysik, Forschungszentrum Karlsruhe, 76021 Karlsruhe, Germany

A. Bercuci, I.M. Brancus, M. Petcu

National Institute of Physics and Nuclear Engineering, 7690 Bucharest, Romania

A. Chilingarian, A. Vardanyan

Cosmic Ray Division, Yerevan Physics Institute, Yerevan 36, Armenia

R. Glasstetter¶), J.R. Hörandel, K.-H. Kampert¶), M. Roth

Institut für experimentelle Kernphysik, Universität Karlsruhe, 76021 Karlsruhe, Germany

A. Risse, J. Zabierowski

Soltan Institute for Nuclear Studies, 90950 Lodz, Poland

Received Nov 30, 2005

The electron and muon number of extensive air showers (EAS) measured at ground level are the main observables of the detector array of the KASCADE experiment. The two-dimensional frequency distribution of these observables is used for reconstructing the energy spectra of five elemental groups representing the chemical composition of primary cosmic rays in the energy range from 10^{15} eV to 10^{17} eV. The results of the presented unfolding analysis depend crucially on simulations of EAS, and therefore on the hadronic interaction models used for their generation. As it turns out, the results for the individual energy spectra show to be sensitive to the characteristics of the interaction model used. Furthermore, none of the models discussed (QGSJet and SIBYLL) is capable to describe the data consistently over the whole measurement range with discrepancies appearing in different energy regions.

PACS: 96.50.sd
Key words: cosmic rays, extensive air showers, energy spectra, hadonic interactions

*) On leave of absence from National Institute of Physics and Nuclear Engineering, Bucharest, Romania
†) Now at University of Leeds, Leeds LS2 9JT, United Kingdom
‡) On leave of absence from Moscow State University, 119899 Moscow, Russia
¶) Now at Fachbereich Physik, Universität Wuppertal, 42097 Wuppertal, Germany

1 Introduction

The energy spectrum of primary cosmic rays follows a simple power law $\mathrm{d}J/\mathrm{d}E \propto E^{\gamma}$ over a large energy range. However, in the energy region around 5 PeV a change of the spectral index γ from $\gamma \approx -2.65$ to $\gamma \approx -3.1$ occurs, the so-called *knee* in the energy spectrum of cosmic rays. Even though the knee feature was discovered [1] nearly 50 years ago, its origin is still not convincingly explained.

The list of possible explanations for the knee is long and is certainly beyond the scope of this paper. For instance, ideas are ranging from astrophysical scenarios, like changing acceleration mechanisms [2, 3, 4], effects due to propagation [5, 6] in the Galaxy, or a single source [7] in our neighbourhood, to particle physics models, proposing interactions for example in the vicinity of the sources [8] or during transport [9], or even postulating new interaction processes taking place in the Earth's atmosphere [10, 11]. For a recent overview on astrophysical models see for example [12] and references therein.

No matter how different the physical approaches to the knee problem may be, all models describe the observed overall (all particle) energy spectrum of cosmic rays. On the other hand, their predictions for the spectral shape of individual energy spectra of elemental groups or even single particle types differ quite strongly, thus providing an opportunity to discriminate between the various models.

As simple as this procedure may look at first glance, as hard is this approach in practice. Due to the low fluxes of cosmic rays above 1 PeV ($\approx 1\ \mathrm{m}^{-2}\mathrm{year}^{-1}\mathrm{sr}^{-1}$) only indirect measurements via the detection of extensive air showers (EAS) induced by primary cosmic particles are feasible. A main property of EAS are their large intrinsic fluctuations, making it even hard to determine spectra of elemental groups. Even worse, each analysis of EAS data has to rely on EAS simulations and therefore on our limited knowledge of particle physics in the energy range of relevance. Since especially the very forward direction of interactions is not accessible in collider experiments, one has to rely on phenomenological interaction models. In some respect these models differ in their predictions strongly, making any analysis concerning individual energy spectra even more difficult.

On the other hand, these dependencies provide an opportunity to test the different hadronic interaction models. Irrespective of the reasonability of the results for the energy spectra the simulations must be capable to describe and reproduce the measured data. Deviations of the simulations from the data can give hints to shortcomings in the models and the underlying physical approaches.

In the following we present an analysis of the classical EAS observables, namely the electron and muon number at ground level (the so-called shower sizes). Due to the high accuracy of the KASCADE experiment the presented method, based on unfolding methods, is capable of reconstructing energy spectra for five elements, representing elemental groups of primary cosmic rays. The analysis is performed using the different high energy hadronic interaction models QGSJet [13] and SIBYLL [14]. In this way the sensitivity of the results to the different interaction models can be shown. Furthermore, it is possible to identify inconsistencies between simulations and data, thus giving hints for further improvement of the interaction models.

2 The KASCADE experiment and the used data

The KASCADE (KArlsruhe Shower Core and Array DEtector) experiment [15], located on the site of the Forschungszentrum Karlsruhe, Germany, is designed for the study of EAS in the primary energy range from 100 TeV to 100 PeV. The experiment is a multi-detector setup, allowing to measure a large number of EAS observables simultaneously. Main detector components are the field array [15], the central detector [16, 17], and the muon tracking detector [18]. In the present analysis only data from the array is used.

The field array consists of 252 detector stations containing shielded and unshielded scintillation detectors, arranged on a square grid of 200×200 m^2 with a spacing of 13 m. The stations are organized in 16 so-called clusters, each one consisting of 16 stations in the outer and 15 stations in the inner part of the array. Figure 1 shows a sketch of the installation and of a detector station.

The array detectors measure the electron and muon densities in the shower separately. For the determination of the electron number N_e and muon number N_μ a fit to the lateral particle densities is performed, using a NKG function [19] for the fit:

$$\rho_{e/\mu}(r) = \frac{\Gamma(4.5-s)}{\Gamma(s)\Gamma(4.5-2s)} \cdot \frac{N_{e/\mu}}{2\pi r^2} \cdot \left(\frac{r}{r_m}\right)^{s-2} \cdot \left(1+\frac{r}{r_m}\right)^{s-4.5} \qquad (1)$$

Here s is a shape parameter describing the steepness of the distribution and r_m a scaling radius. For electrons a value of 89 m and for muons of 420 m for r_m is used. At KASCADE not only the total number of muons is reconstructed, but also the so-called truncated muon number N_μ^{tr}, being the number of muons with

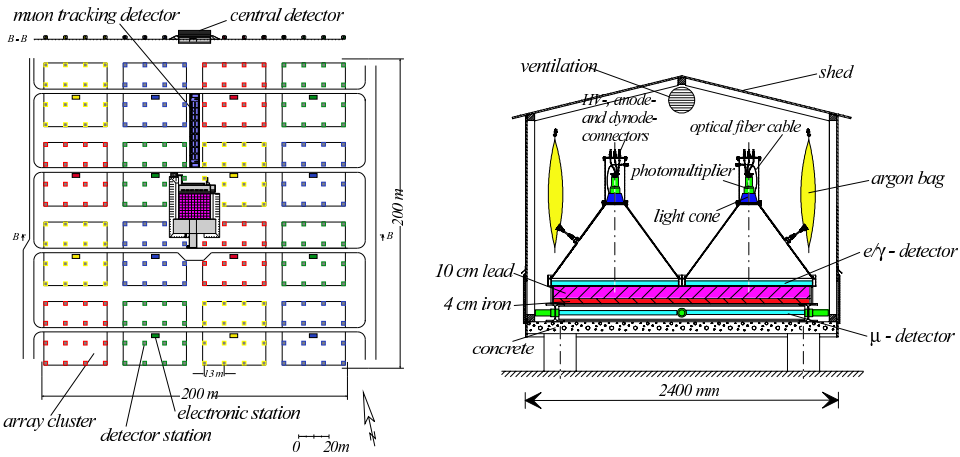

Fig. 1. Left: layout of the KASCADE air shower experiment. Right: sketch of a detector station with shielded and unshielded scintillation detectors.

distances to the shower core between 40 m and 200 m. The restriction to radii larger than 40 m arises from punch through contributions of high energetic electrons and γ-quanta to the muon detector signals close to the shower core.

Input of the analysis is the two-dimensional shower size distribution with respect to the electron number $\lg N_e$ and the truncated muon number $\lg N_\mu^{tr}$. This distribution is displayed in Fig. 2. The zenith angle of the showers used is restricted to values smaller than 18°, the effective measurement time adds up to 900 days. More details about the shower reconstruction algorithms, the data quality, and the applied cuts on the data can be found in [20, 15] and references therein.

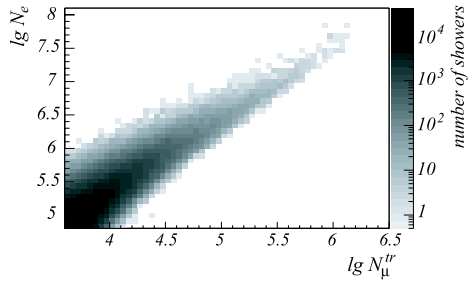

Fig. 2. Two-dimensional shower size spectrum used in the analysis. The range in $\lg N_e$ and $\lg N_\mu^{tr}$ is chosen to avoid influences of inefficiencies.

3 Outline of the analysis

3.1 Notation of the problem

Starting point of the analysis is the two-dimensional shower size spectrum and the contents (number of events) of the corresponding histogram cells displayed in Fig. 2. For simplicity each cell of the histogram is labeled by a single index i for identification. The number of events in each cell i is the superposition of contributions by different primary particles with each possible energy. Thus the relation between the number of showers N_i with shower sizes $(\lg N_e, \lg N_\mu^{tr})_i$ of cell i and the differential fluxes $\mathrm{d}J_A/\mathrm{dlg}\,E$ of primary cosmic ray particles with mass number A can be written as

$$N_i = A_s T_m \sum_{A=1}^{N_A} \int_{-\infty}^{+\infty} \frac{\mathrm{d}J_A}{\mathrm{d}\lg E}\, p_A((\lg N_e, \lg N_\mu^{tr})_i | \lg E)\, \mathrm{d}\lg E \qquad (2)$$

For reasons of clarity an additional integration over solid angle and the corresponding dependencies on azimuth and zenith angle are omitted in Eq. (2) and Eq. (3), but accounted for in the analysis. The conditional probability p_A describes the probability to measure a shower of primary energy $\lg E$ and mass A with shower sizes $(\lg N_e, \lg N_\mu^{tr})_i$. A_S and T_m denote the sampling area and the measurement time, which can be treated as constants in this analysis.

The probability p_A itself is an integral, namely

$$p_A = \int_{-\infty}^{+\infty} \int_{-\infty}^{+\infty} s_A \epsilon_A r_A \, d\lg N_e^{true} \, d\lg N_\mu^{tr,true}. \qquad (3)$$

The distributions $s_A = s_A(\lg N_e^{true}, \lg N_\mu^{tr,true} | \lg E)$ describe the intrinsic shower fluctuations, giving the probability for a shower with primary mass A and energy $\lg E$ to exhibit shower sizes $\lg N_e^{true}$ and $\lg N_\mu^{tr,true}$. The functions $\epsilon_A = \epsilon_A(\lg N_e^{true}, \lg N_\mu^{tr,true})$ represent the detection and reconstruction efficiencies depending on true shower sizes, whereas the properties of the reconstruction are described by the probabilities $r_A = r_A((\lg N_e, \lg N_\mu^{tr})_i | \lg N_e^{true}, \lg N_\mu^{tr,true})$. The latter account for resolution of the reconstruction algorithms and for systematic effects like under- or overestimation of the shower sizes.

3.2 Solution strategy

By use of the notation of Eqs. (2) and (3) the data histogram of Fig. 2 is interpreted as a system of coupled integral equations. The general strategy for solving this system for the energy spectra of elemental groups is the application of unfolding algorithms. For this purpose the equation system is reformulated as matrix equation. This reformulation is straightforward. The calculation of the matrix elements, which correspond to the probabilities of Eq. (2), is performed by means of Monte Carlo simulations (see next paragraph).

A closer inspection of the matrix equation shows, that it is close to singularity and represents an ill-conditioned problem. More details and reasons for these properties are given in [20]. To stabilize the equation system and to accommodate for the limited information content of the measured data, it is necessary to restrict the number of considered primary particle types. For the present analysis five primary particles types are adopted. These are hydrogen (protons), helium, carbon, silicon, and iron. Whereas the spectra of protons and helium will most likely decribe the spectra of single elements, it has to be emphasized that the three other represent only elemental groups and not individual elements. Furthermore, these groups are loosely defined, making it not possible to specify from which elements of these groups the resulting energy spectra stem. This holds especially for the two heavy particle types.

For solving the matrix equation unfolding methods are applied. Three different methods are used in the analysis in order to estimate the systematic uncertainties due to the applied algorithm. These algorithms are the Gold algorithm, unfolding based on the Bayesian theorem, and an entropy based method. Details about the algorithms, their properties, and the application procedures can be found in [20].

3.3 Simulations

For the calculation of the p_A one has to rely on simulations to determine the shower fluctuations, efficiencies, and reconstruction properties. The corresponding simulated distributions are parameterized to simplify numerical integrations. This approach allows also the investigation of the influence of the statistical poorly determined tails of the shower fluctuations.

For the air shower simulations the CORSIKA [21] program with the high energy interaction models QGSJet 01 [13] and SIBYLL 2.1 [14] is used. Low energy inter-

actions are treated with the GHEISHA 2000 [22] code, the electromagnetic part of the shower is simulated using EGS4 [23]. For the determination of efficiencies and reconstruction properties the simulation of the KASCADE experiment is necessary. This simulation is based on a detailed GEANT [24] simulation, the following reconstruction of the showers is done with the standard KASCADE reconstruction software. More details about the simulation and parameterization procedures can be found in [20] and references therein.

4 Results

Unfolding results for the elemental group energy spectra are shown in Fig. 3. In the upper part of the figure results for the spectra of light elements (left) and heavy elements (right) using QGSJet simulations are shown, in the lower part the corresponding spectra using SIBYLL simulations. The shaded bands indicate the systematic (methodical) uncertainties. For low energies (< 10 PeV) these uncer-

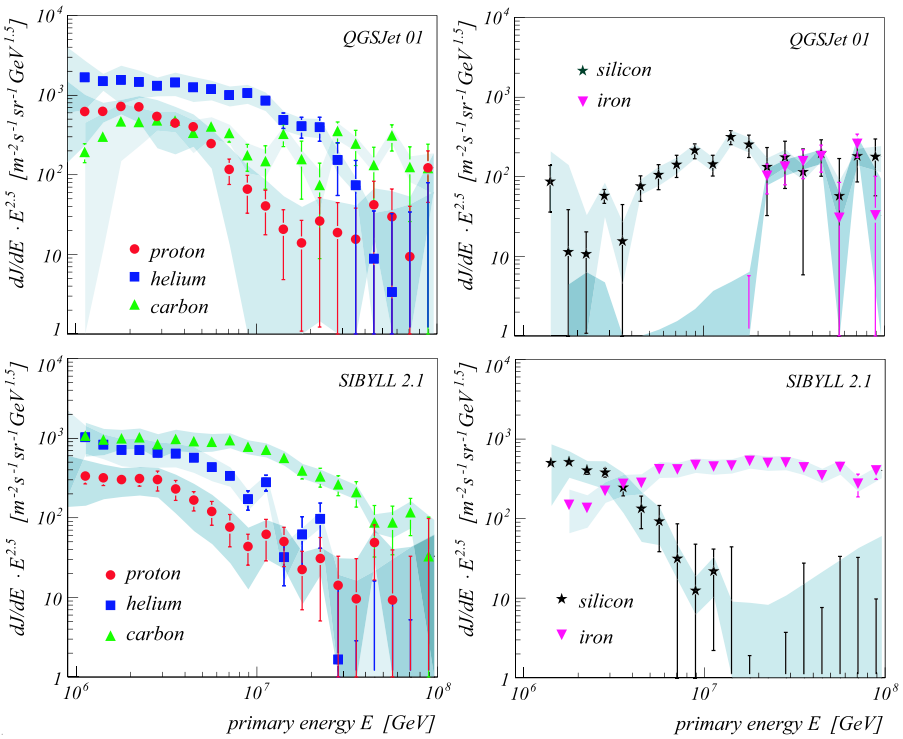

Fig. 3. Results for the energy spectra, H, He, C in left column, Si and Fe in right column. Upper panel: QGSJet01 hypothesis; lower panel: SIBYLL 2.1 hypothesis. The shaded bands indicate methodical uncertainties.

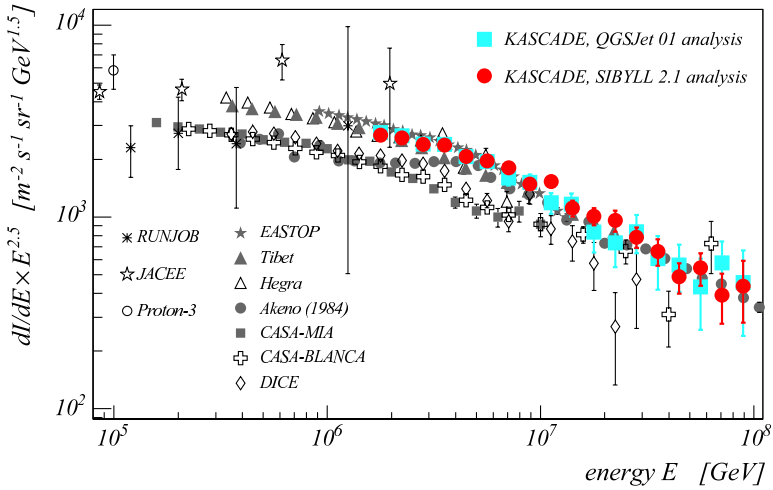

Fig. 4. All particle spectrum for QGSJet and SIBYLL based analysis in comparison with results from some other experiments (taken from [20]).

tainties are dominated by the way the tails of the shower fluctuations s_A are parameterized. At high energies and therefore small number of events the systematic accuracy is limited by the ability of the unfolding algorithms to deal with small statistics.

In the case of the QGSJet based results the composition below the knee is dominated by helium, whereas protons and carbon are a factor of ≈2 less abundant than helium. The proton and the helium spectrum exhibit a knee-like structure, with the position of the helium-knee shifted to higher energy. Beyond each knee the spectra are getting very steep. The spectra of the heavy elements (Si and Fe) look rather unexpected. For energies below 10 PeV practically no iron is present, above 20 PeV it dominates the cosmic ray spectrum together with silicon.

For the SIBYLL based solution the spectra of the light element groups (H, He, C) also exhibit a knee in their spectrum. The position of the individual knees is shifted to higher energies with increasing atomic number. In contrast to the QGSJet results, carbon is the most abundant element at energies around 1-2 PeV, whereas helium is again more abundant than hydrogen. Inside the uncertainties the spectral indices of the light element groups below their knees are the same as for the QGSJet results.

As for the QGSJet results, the spectra of the heavy element groups look unexpected. Silicon is very abundant at energies around 2 PeV, exhibits a knee-like structure at ≈ 3 PeV, and decreases very steeply above. Contrary to silicon, the iron spectrum is very flat, with a slight change of index to $\gamma \approx -2.5$ above 10 PeV.

Common to the results of both interaction models is the occurence of knee-like structures in the spectra of the light primaries (H, He). In the case of the SIBYLL based results even in the carbon spectrum a knee is visible. The “overall picture”

of the cosmic ray energy spectrum around the knee, namely the decrease of light primaries due to knee structures in their energy spectra causing the knee in the all-particle energy spectrum at ≈ 5 PeV, is revealed more or less independently from the used interaction model or unfolding method. Furthermore, the results for the all-particle spectrum of both simulation sets coincide inside their statistical uncertainties, which is displayed in Fig. 4.

5 Description of data

To judge on the properties and the reasonability of the solutions an artifical data set is "constructed" by forward folding of the solution according to Eq. (2). Afterwards a χ^2 test is performed. For the QGSJet based result a value of $\chi^2_{dof} = 2.38$ is found, for the SIBYLL based result a value of $\chi^2_{dof} = 2.46$. The contributions χ^2_i of the individual cells i of the data histogram (see Section 2) to these values are displayed in the upper part of Fig. 5 as a two-dimensional distribution. Strong systematic deviations can be seen in these distribution which occur for the two models in different regions of the data range.

For the QGSJet result (upper part of Fig. 5, left) these deviations are concentrated in the lower part of the measurement range, i.e. at lower energies, with a slight concentration at small electron numbers (for fixed muon number), i.e. showers induced by heavy primaries. For higher energies the data are described well within the statistical uncertainties.

To clarify the nature of these deviations the measured $\lg N_e$-distribution (filled points) for a given interval in $\lg N_\mu^{tr}$ together with the resulting distribution of the forward folding (histogram) is displayed in the lower left part of Fig. 5. The contribution of the different primary types are shown as smooth curves. A large number of showers induced by light elements is needed to describe the tail of the distribution towards large $\lg N_e$. As a consequence, no iron showers are needed for the description of the left-hand tail of the distribution. Even with practically no iron present there are still more showers with $\lg N_e < 5$ calculated than measured. Summarizing, showers generated with QGSJet seem to predict comparatively too little electrons or comparatively too much muons at low energies as required by the data.

In the case of the SIBYLL based result the bulk of the deviations χ^2_i (see upper right part of Fig. 5) is concentrated at medium to high $\lg N_\mu^{tr}$ and small $\lg N_e$ values, i.e. in the region of showers induced by heavy primaries with higher energies. At low energies only small deviations occur. The bad description of the heavy induced shower at higher energies can also be seen in the corresponding $\lg N_e$-distribution for a fixed interval of $\lg N_\mu^{tr}$. In the lower right part of Fig. 5 such a distribution corresponding to the poorly described measurement region is shown. The left-hand tail of the distribution cannot be described using the five assumed particles. In order to fit the distribution the iron contribution is raised nearly to the maximum possible value. Even then the left-hand tail cannot be described. Since the right tail towards larger values of $\lg N_e$ can only be described by lighter elements, there is

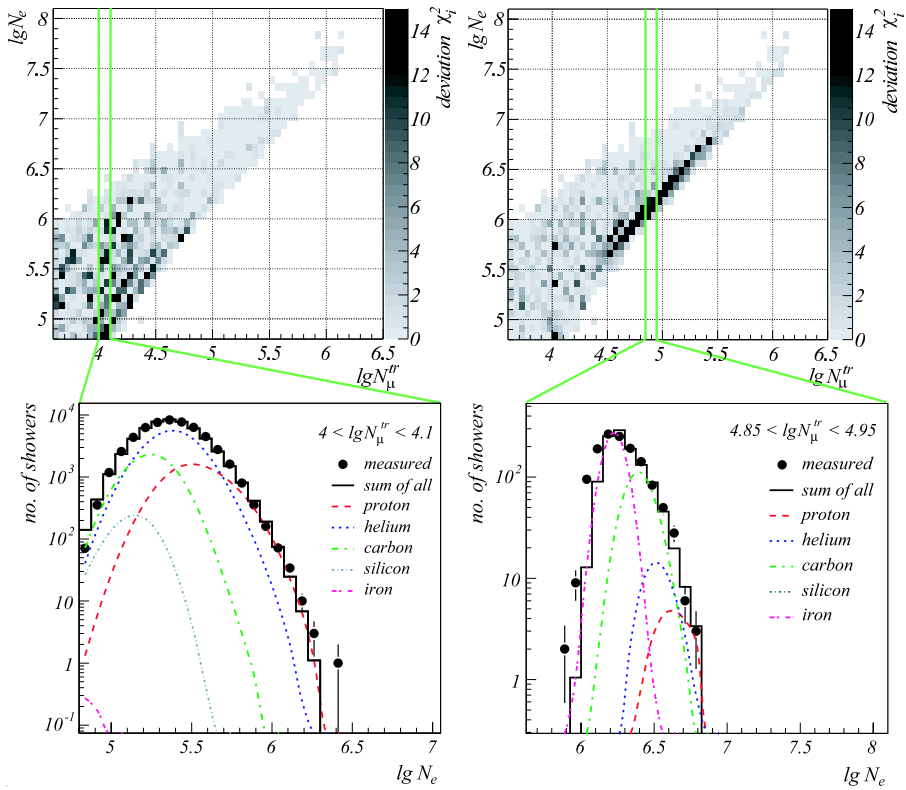

Fig. 5. Upper part: Distribution of deviations between data and forward folded solution for QGSJet (left) and SIBYLL (right). Lower part: Example of insufficient description of measured data for fixed $\lg N_\mu^{tr}$ bins; left panel for QGSJet, right panel for SIBYLL.

no space left for a significant contribution of silicon. This explains the unexpected low-energy knee and the sharp decrease visible in the silicon spectrum of Fig. 3. Showers generated with the SIBYLL model seem to be too electron rich or too muon poor compared to the data.

6 Summary and conclusions

Using the two-dimensional shower size spectrum of electron and muon number measured with the KASCADE experiment an analysis based on unfolding methods was performed. This analysis yielded energy spectra of five primary elements, which represent not single elements but elemental groups and therefore the chemical composition of cosmic rays. Air shower simulations with two different high energy hadronic interaction models were used for the analysis, namely the QGSJet 01 and the SIBYLL 2.1 models. Even though the reconstructed all particle energy spectra

of cosmic rays coincide within the statistical and systematic uncertainties for both simulations sets, the results for the individual element groups differ quite strongly. Furthermore, none of the simulation sets is capable of describing the data over the whole measurement range. For the QGSJet based analysis deviations occur at low energies, whereas for the SIBYLL based analysis higher energies are problematic.

Summarizing, it has been demonstrated that it is possible to reconstruct energy spectra of elemental groups from air shower data, in addition to the all particle spectrum. At present, the limiting factors of the analysis are the properties of the high energy interaction models. On the other hand, it has been shown that the analysis and their results are sensitive to the interaction model used in the simulations. Therefore, the observed discrepancies between the measured data and the simulations can be attributed to the models and may give valuable information for further improvements.

References

[1] G.V. Kulikov, G.B. Khristiansen: Sov. Phys. JETP **51** (1949) 441.

[2] E.G. Berezhko, L.G. Ksenofontov: JETP **89** (1999) 391.

[3] T. Stanev et al.: Astron. Astrophys. **274** (1993) 902.

[4] H.J. Völk, V.N. Zirakashvili: Astron. Astrophys. **417** (2004) 807.

[5] V.S. Ptuskin et al.: Astron. Astrophys. **268** (1993) 726.

[6] J. Candia et al.: JHEP **12** (2002) 033.

[7] A.D. Erlykin, A.W. Wolfendale: J. Phys. G: Nucl. Part. Phys. **23** (1997) 979.

[8] J. Candia et al.: Astropart. Phys. **17** (2002) 23.

[9] R. Wigmans: Astropart. Phys. **19** (2003) 379.

[10] S.I. Nikolsky, V.A. Romachin: Phys. Atomic Nucl. **63** (2000) 1799.

[11] D. Kazanas, A. Nicolaidis: Gen. Rel. Grav. **35** (2003) 1117.

[12] A.D. Erlykin, A.W. Wolfendale: J. Phys. G: Nucl. Part. Phys. (2005) *in press.*

[13] N.N. Kalmykov, S.S. Ostapchenko: Phys. Atom. Nucl. **56** (1993) 346.

[14] R. Engel et al.: Proc. 26th Int. Cosmic Ray Conf. Salt Lake City (USA) **1** (1999) 415.

[15] T. Antoni et al.: Nucl. Instr. Meth. A **513** (2003) 490.

[16] J. Engler et al.: Nucl. Instr. Meth. A **427** (1999) 528.

[17] H. Bozdog et al.: Nucl. Instr. Meth. A **465** (2001) 455.

[18] P. Doll et al.: Nucl. Instr. Meth. A **488** (2002) 517.

[19] K. Greisen: Prog. Cosmic Ray Physics Vol. **III** (1956) 1.

[20] T. Antoni et al.: Astropart. Phys. **24** (2005) 1.

[21] D. Heck et al.: Report FZKA **6019** (1998) Forschungszentrum Karlsruhe.

[22] H. Fesefeldt: Report PITHA **85/02** (1985) RWTH Aachen.

[23] W.R. Nelson et al.: Report SLAC **265** (1985) Stanford Linear Accelerator Center.

[24] GEANT-Detector Description and Simulation Tool: CERN Program Library Long Writeup **W5013** (1993) CERN.